

Gradient carbonyl-iron/carbon-fiber reinforced composite metamaterial for ultra-broadband electromagnetic wave absorption by multi-scale integrated design

Qian Zhou, Tiantian Shi, Bei Xue, Shengyue Gu, Wei Ren, Fang Ye, Xiaomeng Fan, Wenyan Duan, Zihan Zhang, and Lifei Du

Cite this article as:

Qian Zhou, Tiantian Shi, Bei Xue, Shengyue Gu, Wei Ren, Fang Ye, Xiaomeng Fan, Wenyan Duan, Zihan Zhang, and Lifei Du, Gradient carbonyl-iron/carbon-fiber reinforced composite metamaterial for ultra-broadband electromagnetic wave absorption by multi-scale integrated design, *Int. J. Miner. Metall. Mater.*, 30(2023), No. 6, pp. 1198-1206. <https://doi.org/10.1007/s12613-022-2583-4>

View the article online at [SpringerLink](#) or [IJMMM Webpage](#).

Articles you may be interested in

Shu-ling Zhang, Wei-ye Chen, Ning Cui, Qian-qian Wu, and You-liang Su, [Giant magneto impedance effect of Co-rich amorphous fibers under magnetic interaction](#), *Int. J. Miner. Metall. Mater.*, 27(2020), No. 10, pp. 1415-1420. <https://doi.org/10.1007/s12613-020-1968-5>

Zhao-hai Gao, Wei Yu, Xu Chen, Bao-sheng Xie, and Qing-wu Cai, [Effect of gradient temperature rolling process on promoting crack healing in Q500 heavy plates](#), *Int. J. Miner. Metall. Mater.*, 27(2020), No. 3, pp. 354-361. <https://doi.org/10.1007/s12613-019-1855-0>

Ping-hu Chen, Yun Zhang, Rui-qing Li, Yan-xing Liu, and Song-sheng Zeng, [Influence of carbon-partitioning treatment on the microstructure, mechanical properties and wear resistance of *in situ* VCp-reinforced Fe-matrix composite](#), *Int. J. Miner. Metall. Mater.*, 27(2020), No. 1, pp. 100-111. <https://doi.org/10.1007/s12613-019-1909-3>

Ji-wei Bao, Zheng-gen Liu, Man-sheng Chu, Dong Han, Lai-geng Cao, Jun Guo, and Zi-chuan Zhao, [Multi-objective collaborative optimization of metallurgical properties of iron carbon agglomerates using response surface methodology](#), *Int. J. Miner. Metall. Mater.*, 28(2021), No. 12, pp. 1917-1928. <https://doi.org/10.1007/s12613-020-2188-8>

Hao-yang Wang, Xue Cheng, Xiao-feng Li, Ji-min Pan, and Jun-hua Hu, [Coupling effect of the conductivities of Li ions and electrons by introducing LLTO@C fibers in the \$\text{LiNi}_{0.8}\text{Co}_{0.15}\text{Al}_{0.05}\text{O}_2\$ cathode](#), *Int. J. Miner. Metall. Mater.*, 28(2021), No. 2, pp. 305-316. <https://doi.org/10.1007/s12613-020-2145-6>

Muharrem Pul, [Effect of sintering temperature on pore ratio and mechanical properties of composite structure in nano graphene reinforced ZA27 based composites](#), *Int. J. Miner. Metall. Mater.*, 27(2020), No. 2, pp. 232-243. <https://doi.org/10.1007/s12613-019-1926-2>



IJMMM WeChat



QQ author group

Gradient carbonyl-iron/carbon-fiber reinforced composite metamaterial for ultra-broadband electromagnetic wave absorption by multi-scale integrated design

Qian Zhou¹,, Tiantian Shi², Bei Xue¹, Shengyue Gu¹, Wei Ren¹, Fang Ye³, Xiaomeng Fan³, Wenyan Duan⁴, Zihan Zhang¹, and Lifei Du²,

1) College of Science, Xi'an University of Posts and Telecommunications, Xi'an 710121, China

2) College of Materials Science and Engineering, Xi'an University of Science and Technology, Xi'an 710054, China

3) Science and Technology on Thermostructural Composite Materials Laboratory, Northwestern Polytechnical University, Xi'an 710072, China

4) Technology and Engineering Centre for Space Utilisation, Chinese Academy of Sciences, Beijing 100094, China

(Received: 1 October 2022; revised: 5 November 2022; accepted: 2 December 2022)

Abstract: The demand of high-end electromagnetic wave absorbing materials puts forward higher requirements on comprehensive performances of small thickness, lightweight, broadband, and strong absorption. Herein, a novel multi-layer stepped metamaterial absorber with gradient electromagnetic properties is proposed. The complex permittivity and permeability of each layer are tailored via the proportion of carbonyl-iron and carbon-fiber dispersing into the epoxy resin. The proposed metamaterial is further optimized via adjusting the electromagnetic parameters and geometric sizes of each layer. Comparing with the four-layer composite with gradient electromagnetic properties which could only realize reflection loss (RL) of less than -6 dB in 2.0–40 GHz, the optimized stepped metamaterial with the same thickness and electromagnetic properties realizes less than -10 dB in the relevant frequency range. Additionally, the RL of less than -15 dB is achieved in the frequency range of 11.2–21.4 GHz and 28.5–40 GHz. The multiple electromagnetic wave absorption mechanism is discussed based on the experimental and simulation results, which is believed to be attributed to the synergy effect induced by multi-scale structures of the metamaterial. Therefore, combining multi-layer structures and periodic stepped structures into a novel gradient absorbing metamaterial would give new insights into designing microwave absorption devices for broadband electromagnetic protections.

Keywords: broadband absorption; metamaterials; gradient impedance; multi-scale synergic effect

1. Introduction

As a new class of functional materials which is designed for efficiently reducing or eliminating reflected electromagnetic (EM) waves [1–3], absorbing materials are implemented to eliminate adverse EM waves effectively in electronic safety, healthcare, and national defense security [4–5]. For engineering applications, it is also required to have light weight, temperature resistance, corrosion resistance, and other properties, in addition to realizing the efficient absorption in a wide frequency band [6–8]. Traditional EM absorbing materials are mostly homogeneous composites formed by dispersing lossy absorbents in the wave-transparent matrix, and the impedance matching and EM wave loss characteristics are strongly enslaved to the intrinsic EM parameters of the absorbing material [9–10]. Generally, there are two types of lossy absorbents: magnetic lossy absorbents, such as carbonyl iron particles (CIP) [11–12], iron-base alloys [13], and ferrites [14]; dielectric lossy absorbents, such as carbon fibers [15–17], carbon nanotubes (CNTs) [18–19], and graphene [20–22]. However, the high density and the degradation of

magnetic lossy absorbents in the low-frequency range would seriously constrain their applications [23]. Similarly, single-layer homogeneous composites prepared with dielectric lossy absorbents are difficult to realize efficient absorption in a wide frequency range, due to the competition between the impedance matching and electromagnetic losses, since both of which are directly dependent on the EM parameters [24–26].

Therefore, an altered approach is proposed to design an impedance-matched absorbing structure with layers of different EM parameters (multi-layer gradient design): the material with small EM parameters and low loss is placed as the top layer to meet the requirement of impedance matching, and the material with large loss is chosen as the bottom layer to meet the requirements of attenuation for transmitted EM waves [27–29]. For instance, a two-layer polymer-based absorbing composite reinforced by two types of SiC fibers with different electrical resistivity achieved efficient absorption ($>90\%$) in both X and Ku bands [24], and the efficient absorption of another five-layer gradient CNTs/SiO₂ composites enhanced 1.5 times as high as that of the single layer

 Corresponding authors: Qian Zhou E-mail: zhouqian@xupt.edu.cn; Lifei Du E-mail: dulifei@xust.edu.cn

© University of Science and Technology Beijing 2023

CNTs/SiO₂ [30]. Therefore, the impedance matching of the absorbing structures could be significantly improved with the multi-layered structure with gradient EM parameters, which can effectively reduce the harsh requirements to realize the broadband absorbing performances [31–33]. However, the multi-layer structure cannot solve the problem of EM wave absorption in ultra-broadband frequency (such as 2–40 GHz), which limits the critical engineering applications [34].

Another efficient way to improve the impedance matching is the meta-structure design, and the discontinuous three-dimensional (3D) periodic structure design can tailor the equivalent EM properties through the optimization of unit cells, thereby further reducing the relationship between intrinsic EM parameters and impedance matching [35–38]. Furthermore, the periodic array of subwavelength protrusions could realize the regulation of EM waves, which would generate multiple absorption without increasing the thickness of the material, thereby effectively broadening the absorption bandwidth [39–42]. For instance, a 3D reduced graphene oxide sponge metamaterial could achieve the efficient EM wave absorption of 2.4–40 GHz by optimizing the impedance [43]. Therefore, periodic structure design together with the micro-structure design for absorbing materials would excite a synergistic effect with the multi-scale structures, which would broaden the effective absorption bandwidth of the absorbing material with relatively small thickness [34].

It can be seen from the above that both multi-layer and meta-structures could improve the impedance matching characteristics to achieve efficient broadband absorption. Furthermore, there should be more degrees of freedom for macroscopic structure design via combining multilayer structures and periodic structures into a gradient absorbing composite metamaterial (GACM), which would give new insights into broadband microwave absorption. In this paper, the resin-based absorbing composites reinforced with typical spherical CIP and carbon fibers (C_f) were fabricated as intrinsic lossy materials with tunable EM parameters for GACM design. The periodic stepped structure with gradient EM parameters was designed to optimize the absorbing properties, then the four-layered stepped metamaterial absorber was fabricated via the template method. The correlation between the multi-scale structures (including microstructures, layered structures, and periodic structures) and broadband absorbing properties was specified based on the simulated and experimental results. Therefore, the proposed GACM realizes reflection loss (RL) of less than –10 dB in the frequency range of 2.0–40 GHz with a total thickness of 8.0 mm, indicating an ultra-broadband EM absorption, which could be applied as absorbing devices for broadband EM protections.

2. Experimental

2.1. Materials

Spherical CIP were purchased from Zhongmai Metal Material Technology Ltd. China and exhibited a diameter of

5–10 μm with a purity of 98% and the density of 2.45 g/cm³. C_f with an average diameter of 7 μm and the density of 1.76 g/cm³ were supplied by Shanghai Liso Composite Material Technology Co., Ltd., China. The dispersant (9076, BYK Inc., Germany) was selected. The epoxy resin (ER) and its curing agent were purchased from Shenzhen Jinhua Electronic Materials Co. Ltd. China. The defoaming agent (organic silicone, T-2005) was supplied by Foshan Shenghui New Material Co. Ltd. China. All materials are commercially available and used without further purification in this study.

2.2. Fabrication of CIP/C_f/ER composites

In order to achieve the target EM parameters for meta-structural design, the CIP/C_f-reinforced ER absorbing composites were fabricated in ring shapes following the standard of coaxial method. The weight proportion of epoxy resin and curing agent was 100:30. The weight proportions of defoaming agent and dispersant in the resin slurry were 0.01% and 1%, respectively. First, the C_f and dispersant with certain volume fractions were mixed uniformly with hot epoxy resin and defoaming agent, and then vigorously stirred at 100°C for 60 min to remove air bubbles. Second, the CIP with certain volume fractions were added into the above resin mixture to obtain a new uniform mixture. Third, the certain quality hardener was mixed uniformly for 30 min. Finally, the fabricated mixture after vacuum defoaming for 30 min was poured into a flexible silicone resin mould, and insulated at 80°C for 12 h to obtain specimens for EM parameters tests. In order to obtain the EM properties of CIP/C_f/ER composites for gradient absorbing material designed, eight kinds of composite (as shown in Table 1) with different compositions were fabricated and measured.

Table 1. Different volume fractions of CIP and C_f in the fabricated CIP/C_f/ER composites

Sample No.	Component
1#	40vol% CIP + 0.0vol% C _f
2#	45vol% CIP + 0.0vol% C _f
3#	50vol% CIP + 1.7vol% C _f
4#	55vol% CIP + 2.1vol% C _f
5#	57vol% CIP + 0.0vol% C _f
6#	57vol% CIP + 3.3vol% C _f
7#	63vol% CIP + 3.5vol% C _f
8#	65vol% CIP + 2.0vol% C _f

2.3. Fabrication of gradient absorbing composite metamaterial

The proposed gradient absorbing meta-structure consists of a four-layer CIP/C_f/ER composites on the top and the metal backplane at the bottom, which is illustrated in Fig. 1(a). The four types of CIP/C_f/ER (5#, 6#, 7#, and 8#) are selected for the layers after the optimization process. The details of optimization method for EM wave absorption performances are in our previous work [35]. The values of the geometric

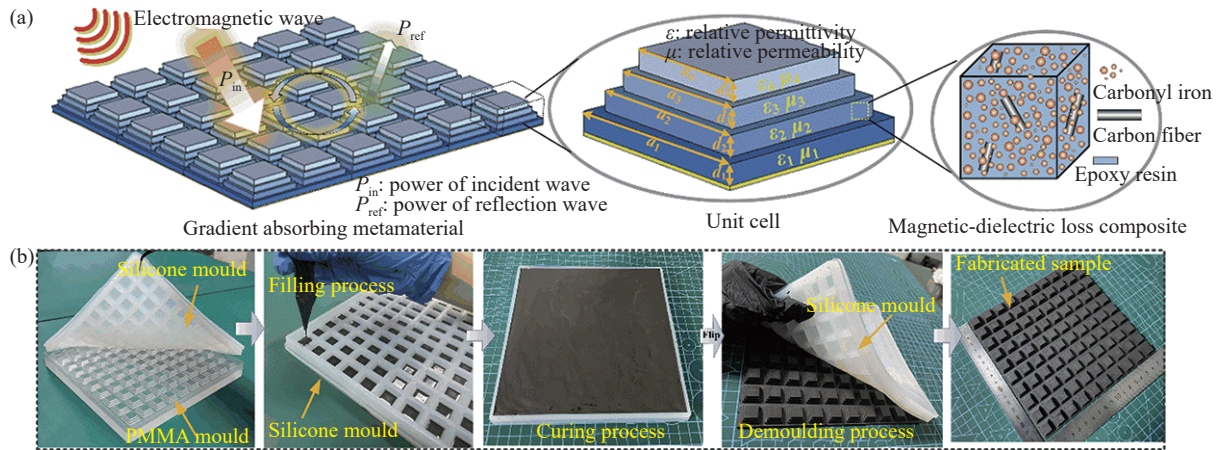


Fig. 1. (a) Schematic of the proposed gradient metamaterial; (b) fabrication process of the proposed gradient absorbing metamaterial.

structure parameters are chosen as follows: $a_1 = 18$ mm, $a_2 = 14$ mm, $a_3 = 12$ mm, $a_4 = 10$ mm, and $d_1 = d_2 = d_3 = d_4 = 2.0$ mm.

In order to verify and test the RL of the designed gradient CIP/C_f/ER metamaterial from 2 to 40 GHz, a structural plate of 180 mm × 180 mm × 8 mm was fabricated with a two-step molding method, which is given in Fig. 1(b). First, the polymethyl methacrylate (PMMA) mould with corresponding sizes was manufactured by high precision numerically controlled machining. Second, the flexible female silicone mould was achieved via pouring the liquid high temperature silicone after vacuum defoaming and curing in the above male PMMA mould at room temperature for 5 h. Third, the certain content mixture of CIP/C_f/ER were poured carefully into the silicone mould layer to fill the first layer, and then cured at 100°C for 12 h. Then, the above procedure was repeated to fill the other three layers and complete the curing process. Finally, the gradient CIP/C_f/ER metamaterial was obtained by demoulding process.

2.4. Characterization and measurements

Microstructure observations and analysis of the CIP/C_f/ER composites were performed by using field-emission scanning electron microscopy (SEM, Jeol, JSM-7610FPlus). The complex permeability and permittivity of CIP/C_f/ER composites were determined by a vector network analyzer (VNA, N5234A) with the coaxial test method (outer diameter of 7 mm, inner diameter of 3 mm, and thickness of 3 mm) from 2 to 18 GHz. The RL of the prepared GACM was measured by the arch frame test system with two broadband horn antennas connected to two ports of the VNA (MS4644A; Japan), with the emitting and receiving EM wave signals in 2–40 GHz. CST Microwave Studio was used to simulate the RL, EM field distribution, and power loss of the designed GACM.

3. Results and discussion

3.1. Properties of CIP/C_f/ER composites

Fig. 2(a) and (b) shows the original morphology of CIP and C_f. In Fig. 2(c), CIP and C_f are evenly dispersed in the epoxy resin, and the morphology of CIP and C_f is similar to

the original state in Fig. 2(a) and (b), and the epoxy fills into the gaps between CIP and C_f. The measured relative complex permeability ($\mu = \mu' - j\mu''$) and permittivity ($\epsilon = \epsilon' - j\epsilon''$) of CIP/C_f/ER composites are shown in Fig. 2(d) and (e). For all samples, the values of the real part of relative permeability and imaginary part of relative permittivity change relatively small, while the values of the imaginary part of relative permeability and real part of relative permittivity change greatly. Comparing the specimens of 1# and 2# (6# and 7#), the imaginary part of permeability increases greatly, but the imaginary part of permittivity slightly changes with the increase of CIP content. As the increase of C_f content, the imaginary part of permittivity increases obviously by comparing the specimens of 3# and 4# (5# and 6#). It is shown that CIP mainly regulates magnetic loss while C_f mainly regulates dielectric loss. This is because the charge movement, which is induced by the conductive network formed with C_f in the alternating electromagnetic field, produces a reverse induced magnetic field to reduce the magnetic loss ability. By introducing these two kinds of EM wave absorbing agents, the frequency-dependent permeability and permittivity of the CIP/C_f/ER composites can be adjusted effectively. The decreased real part of permeability with increasing frequency should be caused by the domain-wall motion and relaxation in CIP, while the decreased imaginary part should be the result of the natural resonance and eddy-current loss in CIP. The less variation of real part in permittivity could be due to the fact that the polarization of the dielectric dipoles is in phase with the oscillation of the electric field vector of the transverse electromagnetic wave, while the increased imaginary part with increasing frequency could be the result of the relaxation polarization and electric conductance during the oscillation of the dipoles in the high-frequency range [12]. Therefore, The gradient variation of EM parameters provides more choosabilities for designing multi-layer absorbing materials.

Based on the transmission line theory and metal back-plane model, the RL of absorbing materials can be calculated by its permeability (μ), permittivity (ϵ), and thickness (d) [44]:

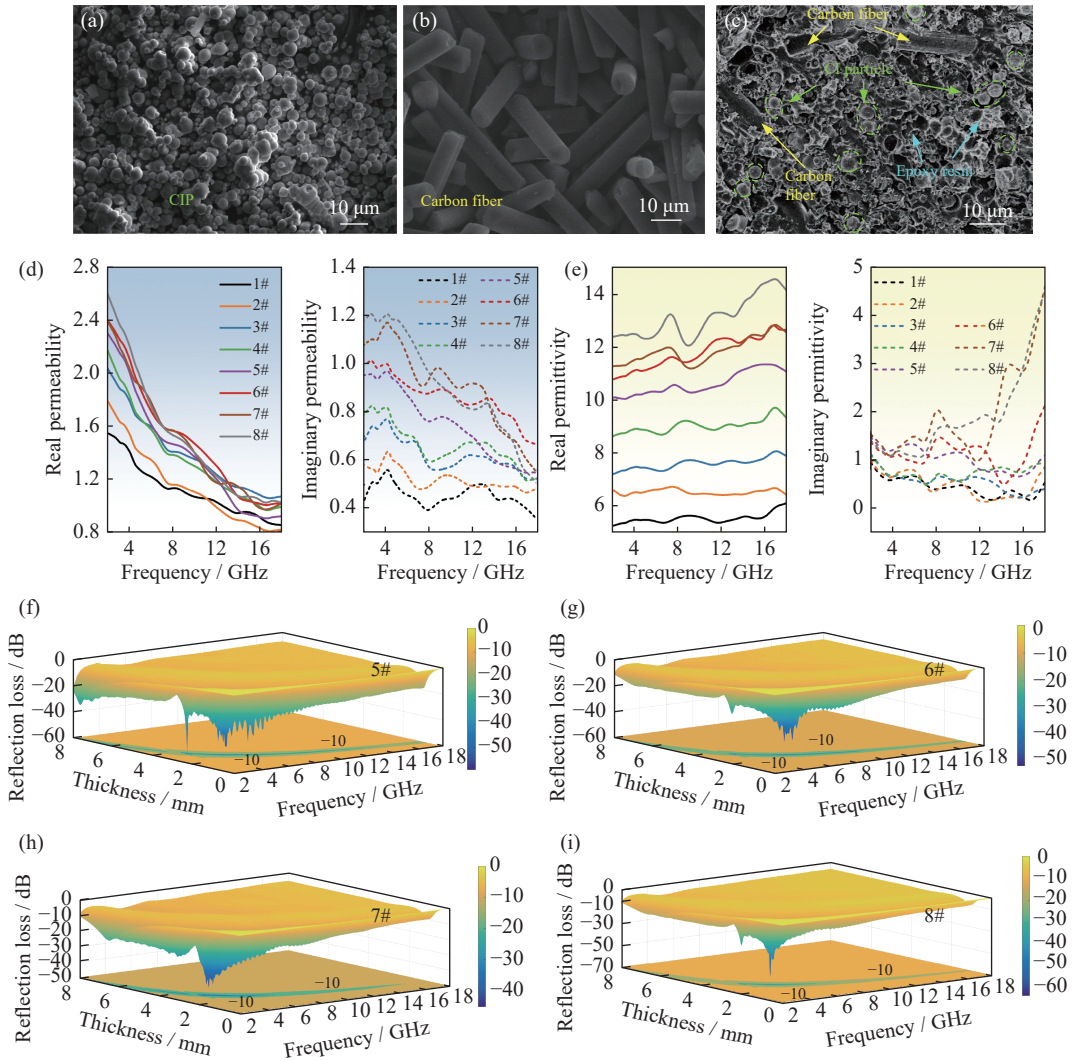


Fig. 2. (a) Original morphology of CIP; (b) original morphology of C_f; (c) the distribution of CIP and C_f in the ER matrix. (d, e) Complex permeability and permittivity of CIP/C_f/ER composites. (f)–(i) 3D distribution map of RL with thickness (*d*) and frequency (f) for the single layer CIP/C_f/ER composites with different CIP and C_f contents.

$$Z_{in} = Z_0 \sqrt{\frac{\mu}{\varepsilon}} \tanh\left(j \frac{2\pi f d \sqrt{\varepsilon\mu}}{c}\right) \quad (1)$$

$$RL = 20 \lg \left| \frac{Z_{in} - Z_0}{Z_{in} + Z_0} \right| \quad (\text{dB}) \quad (2)$$

where Z_0 is the characteristic impedance of free space, Z_{in} is the input impedance at the interface between the air and absorbing material, f is the frequency of EM wave, and c represents the speed of light in the free space. The theoretical RL for single layer absorbing materials with respect to frequency and thickness can be calculated through Eqs. (1) and (2). As shown in Fig. 2(f)–(i), these single-layer CIP/C_f/ER composites only show strong EM wave absorption at certain frequency points with a certain thickness, and these absorption peaks come from $n/4$ ($n = 1, 2, 3, 4, \dots$) wavelength resonance [45]. Obviously, without macro structural design, it is difficult to achieve broadband absorption by simply adjusting permittivity and permeability [46]. Therefore, it is necessary to design multilayer and metamaterial at macro scale on the basis of the above material microstructure design to achieve ultra-broadband EM wave absorption.

3.2. Gradient CIP/C_f/ER composite metamaterial

CST simulation optimization was carried out to achieve the maximum broadband EM wave absorption under the minimum thickness. The effective absorption bandwidth (EAB) with RL less than -10 dB ($>90\%$ absorption) and strong absorption intensity were taken as targets for material selection for each layer and the optimization of geometric structure parameters. Fig. S1(a) and (b) shows the simulated RL curves of gradient structure and gradient metamaterial structure under different material combinations. The RL curves for different geometric structure parameters are shown in the Fig. S2(a)–(f). The material types and geometric structure parameters of each layer for the final optimized structure are shown in Table S1. Fig. 3(a) gives the RL curves of optimized four-layer gradient composite and gradient composite metamaterial. The RL value is almost less than -10 dB in the 2–40 GHz frequency for the GACM, while the RL value of the four-layer gradient composite is only less than -6 dB. The contribution of each layer of the gradient metamaterial on the rate of power loss calculated via the CST simulation is

plotted in Fig. 3(b). The layer-1 at the bottom contributes the largest absorption in relative lower frequency band (about 2–10 GHz) of EM waves, and realizes more than 52.6% absorption at 3.2 GHz. Different from the bottom absorbing layer-1, the layer-4 on the top contributes the largest absorption in relative higher frequency band (about 20–36 GHz) of EM waves. Similarly, the middle layer near the bottom (layer-2) shows large EM wave absorption at relatively low frequencies, while the middle layer near the top (layer-3) has strong EM wave absorption at relatively high frequencies. The EM wave absorption of the layer-3 is about 30% in the whole 6–40 GHz frequency band. Therefore, the designed four-layer gradient metamaterial could realize the ultra-broadband EM waves absorption (more than 90% absorption band is 38 GHz in the frequency range of 2–40 GHz).

The normalized complex input impedance can be obtained from the simulated complex parameters of S_{11} and S_{21} by the effective medium theory [47] and the result was plotted in Fig. 3(c) and (d):

$$Z(f) = \sqrt{\frac{\mu_{\text{eff}}}{\varepsilon_{\text{eff}}}} = \sqrt{\frac{(1+S_{11})^2 - S_{21}^2}{(1-S_{11})^2 - S_{21}^2}} \quad (3)$$

The improved absorption efficiency of the designed metamaterial absorber could be mainly attributed to two aspects: (1) the non-continuous periodic stepped meta-structure can further improve the impedance matching, resulting in less reflection of the EM wave at the surface of the metamaterial; (2) the multiple loss mode induced by the

multi-scale structure, such as coupling effect between unit cells and multiple resonance induced by electromagnetic interfaces of the meta-structure, can effectively attenuate the transmitted EM wave, resulting in less secondary reflection for the EM wave [43].

The electric field, magnetic field, and power loss density distributions at four significant resonant frequency peaks (3.12, 13.6, 24.6, and 39.8 GHz) were calculated to further understand the mechanism of absorption behaviors in the proposed metamaterial, and the results are shown in Fig. 4. For the first absorption peak at 3.12 GHz (Fig. 4(a)), the electric field distribution is mainly concentrated on the outside of the metamaterial structure along the y direction (direction of the electric field), and the magnetic field mainly focuses on the bottom middle of the metamaterial plate. Major power loss takes place on the bottom of the structure which coincides with magnetic field concentration areas, and shows a typical complex ferromagnetic resonance and $\lambda/4$ resonance characteristics [42]. When the frequency increased to 13.6 GHz (Fig. 4(b)), their modulus of electric field $|E|$, modulus of magnetic field $|H|$, and power loss distributions are all similar, which is mainly aggregated in the top and trapezoidal shell region of the meta-structure. For the higher frequency peaks at 24.6 GHz and 39.8 GHz (Fig. 4(c) and (d)), electric field, magnetic field, and power loss distributions are all mainly occurred in the trapezoidal shell region of the meta-structure. With the increase of frequency, the electromagnetic field distribution and power loss distribution gradually

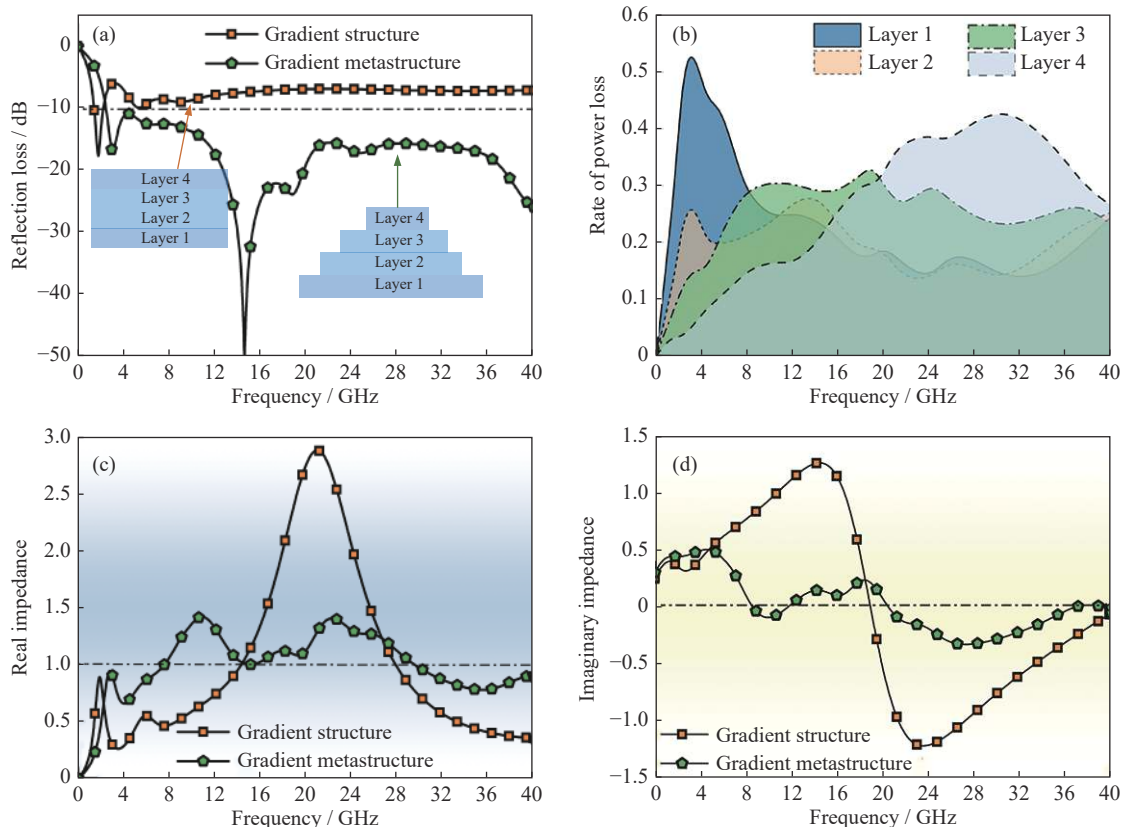


Fig. 3. (a) RL curves of four-layer gradient CIP/C_r/ER composite and gradient CIP/C_r/ER metamaterial; (b) the contribution of each layer of the gradient CIP/C_r/ER metamaterial to the rate of power loss. Complex impedance spectra of gradient multilayer structure and gradient metamaterial: (c) real part; (d) imaginary part.

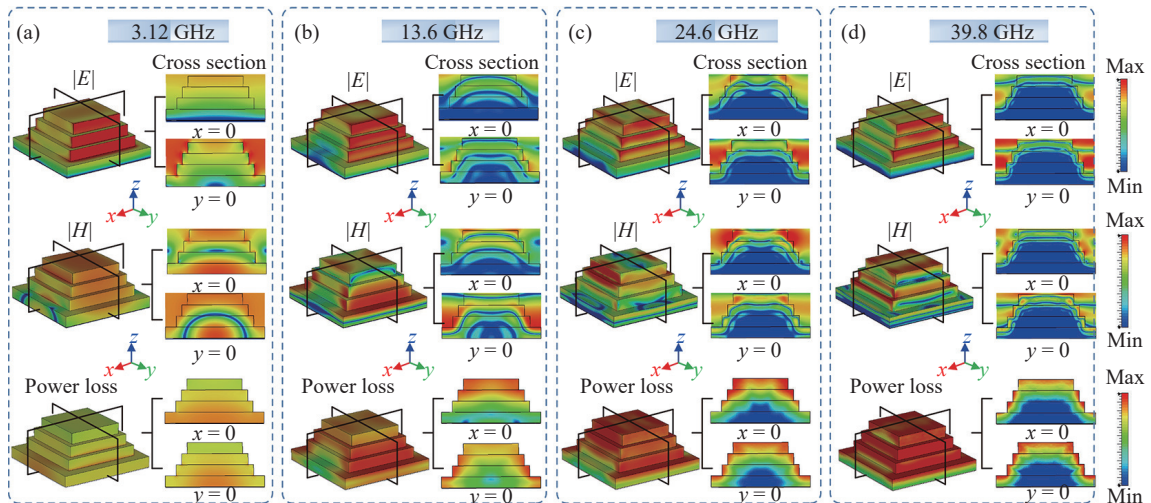


Fig. 4. Distribution of electric field, magnetic field, and power loss density of the proposed CIP/C_f/ER composite meta-structure at different absorption peak frequencies: (a) 3.12 GHz; (b) 13.6 GHz; (c) 24.6 GHz; (d) 39.8 GHz.

shift from the bottom and inside of the material to the shell regions. The higher the frequency, the closer it is to the shell. In addition, with the increase of frequency, the electric field distribution is more similar to the power loss distribution, indicating that the electric loss plays an increasingly obvious role in the total power loss, which is related to the increase of the imaginary part of the permittivity of the CIP/C_f/ER composites at high frequency as shown in Fig. 2. Therefore, the

incorporation of the meta-structure of the gradient absorbing material would result in the enhanced power loss in a broadband frequency, leading to a broadband electromagnetic wave absorbing capacity.

In order to validate the combination design of multilayer gradient structure and the stepped metamaterial, the corresponding CIP/C_f/ER GACM was prepared. Fig. 5(a) shows the fabricated sample and the test diagram of the segmental

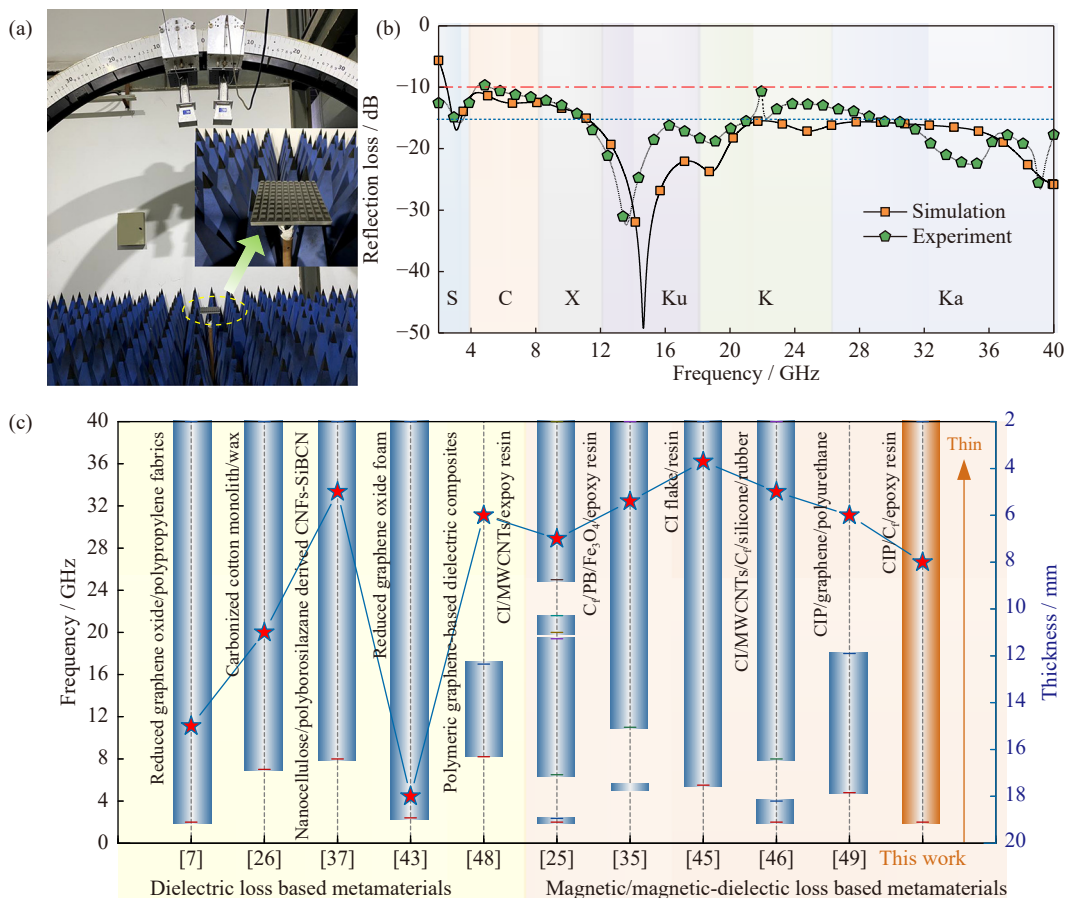


Fig. 5. (a) Photographs of the fabricated sample and the test diagram of the segmental support method; (b) RL curves of the experimental and simulation results; (c) comparison of below -10 dB RL frequency bands and thicknesses for dielectric loss based and magnetic/magnetic-dielectric loss based absorbing metamaterials in reported literatures.

support RL method. Fig. 5(b) gives the measured and simulated RL curves of the optimized metamaterial. The prepared GACM with the total thickness of 8.0 mm realizes less than -10 dB RL in 2.0–40 GHz, indicating an ultra-broadband EM absorption, that is the more than 90% effective absorption bandwidth covers the whole six frequency bands (S, C, X, Ku, K, and Ka bands). In addition, the experimental RL covers -15 dB absorption bandwidth in frequency ranges of 11.2–21.4 GHz and 28.5–40 GHz. Therefore, the proposed gradient metamaterial design methodology is effective to obtain broadband EM wave absorbing materials. As shown in Fig. 5(c), the designed GACM possesses the advantages of both broadband absorption properties and thin thickness, compared with other dielectric loss [7,26,37,43,48] based and magnetic/magnetic-dielectric loss [25,42,45–46,49] based absorbing metamaterials in reported literatures. Generally, dielectric lossy metamaterials usually have the small density with a large thickness, while magnetic lossy and dielectric cooperative lossy metamaterials usually have the small thickness. The proposed GACM achieves strong absorption (RL less than -10 dB) in full-band of 2–40 GHz, which is much better than the bandwidth of other metamaterials, as shown in Fig. 5(c).

The realization of strong and broadband absorption performance by the designed GACM can be mainly attributed to its multiscale and multiple EM wave absorption mechanism, which is summarized in the Fig. 6. On one hand, the combin-

ation of multilayer gradient structure and periodic structure leads to excellent impedance matching properties in broadband frequency. As shown in Fig. 3(c) and (d), comparing with the four-layer gradient composite, the real part of impedance of the designed GACM is more close to unity while imaginary part is more close to zero for all frequency band. This well impedance matching could reduce the primary backward reflection of the EM wave at the surface of the designed metamaterial [35,40], which promotes EM wave to enter into material for further dissipation as shown in Fig. 6(a). On the other hand, multi-scale structure design can produce multiple EM wave loss behavior in different scales, so that the EM wave entering the material is almost consumed. For the macroscopic scale, magnetic field convergence effect and coupling resonance of the stepped meta-structures would be dominated with dispersed CIP and C_f in ER matrix. Metamaterial structures can excite multiple EM resonance between periodic structures at different frequencies, and multilayer structure shows multiple EM interference, as indicated in Fig. 6(b) and (c). At the microscopic scale, the intrinsic losses of CIP/ C_f /ER composite include magnetic losses caused by CIP and dielectric losses caused by C_f occurring (Fig. 6(d)–(f)). Both the magnetic loss of nature resonance, eddy current, and exchange resonances generated from CIP and the conductance loss, dipole polarization, and interfacial polarization coming from C_f are sufficient factors for its EM wave dissipation. Additionally, the

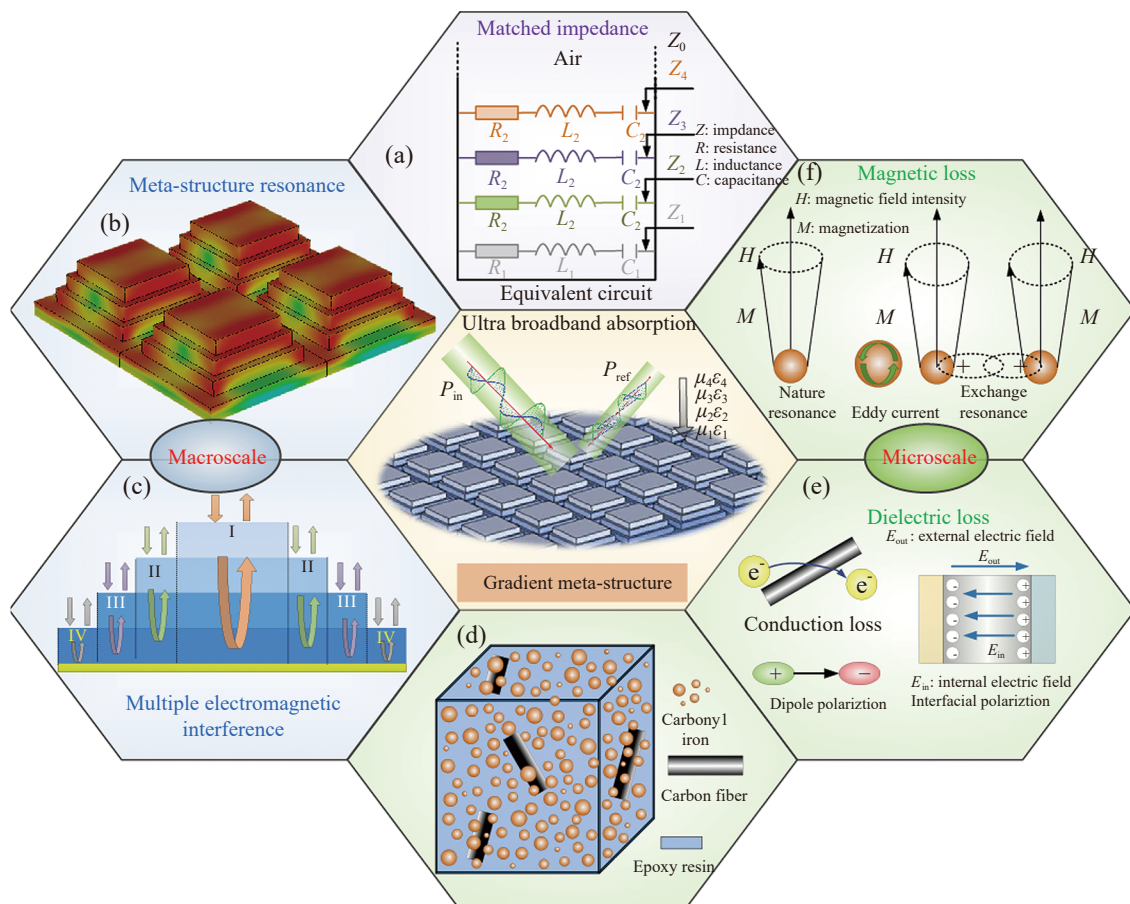


Fig. 6. Schematic of EM wave absorption mechanism of the proposed gradient absorbing metamaterial: (a) the matched impedance; (b, c) the electromagnetic loss in macroscopic scale; (d)–(f) the electromagnetic loss in microscopic scale.

dielectric losses of the CIP/C_f/ER composite caused by C_f with conductive loss as well as dielectric polarization effects and extra multiple reflections induced by numerous mesoscopic interfaces in the CIP/C_f/ER composite would also enhance the attenuation capacity of the metamaterial absorber [49–50]. Therefore, the combination of multilayer gradient structure and periodic structure could significantly improve the impedance matching of the metamaterial, and the strong attenuation of EM wave is mainly attributed to the synergy effect of multiple EM wave absorption mechanisms caused by multi-scale structures.

4. Conclusions

The critical requirement for EM wave absorbing materials is to realize more than 90% absorption in the broader range of operating frequencies. In this study, a novel multi-layered stepped metamaterial is designed and fabricated via combing the multilayer structure and periodic stepped structure. Based on the complex relative permeability and permittivity of CIP/C_f/ER composites, the geometric parameters of the multi-layered periodic stepped structure were optimized, and a four-layer absorbing metamaterial with a total thickness of 8.0 mm was proposed and fabricated. The prepared sample achieved an ultra-broadband EM wave absorption, which realized less than -10 dB RL in the range of 2.0–40 GHz, covering the whole S, C, X, Ku, K, and Ka frequency bands. Additionally, the experimental RL covers -15 dB absorption bandwidth in the frequency ranges of 11.2–21.4 GHz and 28.5–40 GHz. The impedance matching of the designed absorbing metamaterial was significantly improved via combining the multilayer gradient structure and periodic stepped structure, and the strong attenuation of EM wave should be mainly attributed to the synergic effect of multiple EM wave absorption mechanisms caused by multi-scale structures. Therefore, the proposed GACM shows an ultra-broadband EM absorption property with a relatively small thickness, which could be applied as absorbing devices for broadband EM protections.

Acknowledgements

This work was financially supported by the National Natural Science Foundation of China (No. 52102113), the Nature Science Foundation of Shaanxi in China (No. 2022JQ-323), the Creative Research Foundation of the Science and Technology on Thermostructural Composite Materials Laboratory, and the Natural Science Foundation and Department of Education of Shaanxi in China (No. 21JK0912).

Conflict of Interest

The authors declare that they have no known competing financial interests or personal relationships that could have appeared to influence the work reported in this paper.

Supplementary Information

The online version contains supplementary material available at <https://doi.org/10.1007/s12613-022-2583-4>.

References

- [1] Z. Zhang, H.S. Lei, H.Y. Yang, *et al.*, Novel multifunctional lattice composite structures with superior load-bearing capacities and radar absorption characteristics, *Compos. Sci. Technol.*, 216(2021), art. No. 109064.
- [2] J. Liang, F. Ye, Y.C. Cao, R. Mo, L.F. Cheng, and Q. Song, Defect-engineered graphene/Si₃N₄ multilayer alternating core-shell nanowire membrane: A plainified hybrid for broadband electromagnetic wave absorption, *Adv. Funct. Mater.*, 32(2022), No. 22, art. No. 2200141.
- [3] M.H. Li, W.J. Zhu, X. Li, *et al.*, Ti₃C₂T_x/MoS₂ self-rolling rod-based foam boosts interfacial polarization for electromagnetic wave absorption, *Adv. Sci.*, 9(2022), No. 16, art. No. 2201118.
- [4] Q.F. Fan, Y.X. Huang, M.J. Chen, Y. Li, W.L. Song, and D.N. Fang, Integrated design of component and configuration for a flexible and ultrabroadband radar absorbing composite, *Compos. Sci. Technol.*, 176(2019), p. 81.
- [5] T.J. Cui, Microwave metamaterials, *Natl. Sci. Rev.*, 5(2018), No. 2, p. 134.
- [6] X.W. Yin, L.F. Cheng, L.T. Zhang, N. Travitzky, and P. Greil, Fibre-reinforced multifunctional SiC matrix composite materials, *Int. Mater. Rev.*, 62(2017), No. 3, p. 117.
- [7] X. Li, X.K. Lu, M.H. Li, *et al.*, A SiC nanowires/Ba_{0.75}Sr_{0.25}Al₂Si₂O₈ ceramic heterojunction for stable electromagnetic absorption under variable-temperature, *J. Mater. Sci. Technol.*, 125(2022), p. 29.
- [8] P. Zhou, J.H. Chen, M. Liu, P. Jiang, B. Li, and X.M. Hou, Microwave absorption properties of SiC@SiO₂@Fe₃O₄ hybrids in the 2–18 GHz range, *Int. J. Miner. Metall. Mater.*, 24(2017), No. 7, p. 804.
- [9] Q. Zhou, X.W. Yin, F. Ye, *et al.*, Multiscale designed SiC_f/Si₃N₄ composite for low and high frequency cooperative electromagnetic absorption, *J. Am. Ceram. Soc.*, 101(2018), No. 12, p. 5552.
- [10] W.Y. Duan, X.W. Yin, Q. Li, X.M. Liu, L.F. Cheng, and L.T. Zhang, Synthesis and microwave absorption properties of SiC nanowires reinforced SiOC ceramic, *J. Eur. Ceram. Soc.*, 34(2014), No. 2, p. 257.
- [11] M. Yu, P.G. Yang, J. Fu, and S.Z. Liu, Flower-like carbonyl iron powder modified by nanoflakes: Preparation and microwave absorption properties, *Appl. Phys. Lett.*, 106(2015), No. 16, art. No. 161904.
- [12] Y.P. Duan, G.L. Wu, S.C. Gu, S.Q. Li, and G.J. Ma, Study on microwave absorbing properties of carbonyl-iron composite coating based on PVC and Al sheet, *Appl. Surf. Sci.*, 258(2012), No. 15, p. 5746.
- [13] H. Li, Z.M. Cao, J.Y. Lin, *et al.*, Synthesis of u-channelled spherical Fe_x(Co_yNi_{1-y})_{100-x} Janus colloidal particles with excellent electromagnetic wave absorption performance, *Nanoscale*, 10(2018), No. 4, p. 1930.
- [14] P.F. Yin, G.L. Wu, Y.T. Tang, *et al.*, Structure regulation in N-doping biconical carbon frame decorated with CoFe₂O₄ and (Fe,Ni) for broadband microwave absorption, *Chem. Eng. J.*, 446(2022), art. No. 136975.
- [15] Y.Q. Pang, Y.F. Li, J.F. Wang, *et al.*, Carbon fiber assisted glass fabric composite materials for broadband radar cross section reduction, *Compos. Sci. Technol.*, 158(2018), p. 19.
- [16] I.M.D. Rosa, A. Dinescu, F. Sarasini, M.S. Sarto, and A. Tamburrano, Effect of short carbon fibers and MWCNTs on microwave absorbing properties of polyester composites containing nickel-coated carbon fibers, *Compos. Sci. Technol.*,

- 70(2010), No. 1, p. 102.
- [17] Y. Luo, D. Estevez, F. Scarpa, *et al.*, Microwave properties of metamaterials containing carbon fibres and ferromagnetic microwires, *Research*, 2019(2019), art. No. 3239879.
- [18] L. Kong, S.H. Luo, G.Q. Zhang, *et al.*, Interfacial polarization dominant CNTs/PyC hollow microspheres as a lightweight electromagnetic wave absorbing material, *Carbon*, 193(2022), p. 216.
- [19] X.X. Bai, X.J. Hu, S.Y. Zhou, L.F. Li, and M. Rohwerder, Controllable synthesis of leaflet-like poly (3,4-ethylenedioxythiophene)/single-walled carbon nanotube composites with microwave absorbing property, *Compos. Sci. Technol.*, 110(2015), p. 166.
- [20] F. Ye, Q. Song, Z.C. Zhang, *et al.*, Direct growth of edge-rich graphene with tunable dielectric properties in porous Si₃N₄ ceramic for broadband high-performance microwave absorption, *Adv. Funct. Mater.*, 28(2018), No. 17, art. No. 1707205.
- [21] C.Q. Song, X.W. Yin, M.K. Han, *et al.*, Three-dimensional reduced graphene oxide foam modified with ZnO nanowires for enhanced microwave absorption properties, *Carbon*, 116(2017), p. 50.
- [22] L.Z. Wu, R.W. Shu, J.B. Zhang, and X.T. Chen, Synthesis of three-dimensional porous netlike nitrogen-doped reduced graphene oxide/cerium oxide composite aerogels towards high-efficiency microwave absorption, *J. Colloid Interface Sci.*, 608(2022), p. 1212.
- [23] X.P. Li, Z.M. Deng, Y. Li, *et al.*, Controllable synthesis of hollow microspheres with Fe@carbon dual-shells for broad bandwidth microwave absorption, *Carbon*, 147(2019), p. 172.
- [24] Q. Zhou, X.W. Yin, H.L. Xu, *et al.*, Design and fabrication of silicon carbides reinforced composite with excellent radar absorption property in X and Ku band, *J. Phys. D: Appl. Phys.*, 52(2019), No. 43, art. No. 435102.
- [25] Y.X. Huang, W.L. Song, C.X. Wang, *et al.*, Multi-scale design of electromagnetic composite metamaterials for broadband microwave absorption, *Compos. Sci. Technol.*, 162(2018), p. 206.
- [26] W.L. Song, Z.L. Zhou, L.C. Wang, *et al.*, Constructing repairable meta-structures of ultra-broad-band electromagnetic absorption from three-dimensional printed patterned shells, *ACS Appl. Mater. Interfaces*, 9(2017), No. 49, p. 43179.
- [27] D. Micheli, R. Pastore, A. Delfini, *et al.*, Electromagnetic characterization of advanced nanostructured materials and multilayer design optimization for metrological and low radar observability applications, *Acta Astronaut.*, 134(2017), p. 33.
- [28] Y. Liu, X.X. Liu, and X.J. Wang, Double-layer microwave absorber based on CoFe₂O₄ ferrite and carbonyl iron composites, *J. Alloys Compd.*, 584(2014), p. 249.
- [29] X.Y. Gao, J. Li, Y. Gao, S.Y. Guo, H. Wu, and R. Chen, Microwave absorbing properties of alternating multilayer composites consisting of poly (vinyl chloride) and multi-walled carbon nanotube filled poly (vinyl chloride) layers, *Compos. Sci. Technol.*, 130(2016), p. 10.
- [30] M.X. Chen, Y. Zhu, Y.B. Pan, H.M. Kou, H. Xu, and J.K. Guo, Gradient multilayer structural design of CNTs/SiO₂ composites for improving microwave absorbing properties, *Mater. Des.*, 32(2011), No. 5, p. 3013.
- [31] A. Shah, A. Ding, Y.H. Wang, *et al.*, Enhanced microwave absorption by arrayed carbon fibers and gradient dispersion of Fe nanoparticles in epoxy resin composites, *Carbon*, 96(2016), p. 987.
- [32] Y. Gao, X.Y. Gao, J. Li, and S.Y. Guo, Microwave absorbing and mechanical properties of alternating multilayer carbonyl iron powder-poly(vinyl chloride) composites, *J. Appl. Polym. Sci.*, 135(2018), No. 12, art. No. 45846.
- [33] J.P. Gogoi and N.S. Bhattacharyya, Expanded graphite—Phenolic resin composites based double layer microwave absorber for X-band applications, *J. Appl. Phys.*, 116(2014), No. 20, art. No. 204101.
- [34] Q.F. Fan, X.Z. Yang, H.S. Lei, Y.Y. Liu, Y.X. Huang, and M.J. Chen, Gradient nanocomposite with metastructure design for broadband radar absorption, *Composites Part A*, 129(2020), art. No. 105698.
- [35] Q. Zhou, X.W. Yin, F. Ye, X.F. Liu, L.F. Cheng, and L.T. Zhang, A novel two-layer periodic stepped structure for effective broadband radar electromagnetic absorption, *Mater. Des.*, 123(2017), p. 46.
- [36] P.T. Xie, Z.D. Zhang, Z.Y. Wang, K. Sun, and R.H. Fan, Targeted double negative properties in silver/silica random metamaterials by precise control of microstructures, *Research*, 2019(2019), art. No. 1021368.
- [37] H.Q. Liu, Y.B. Zhang, X.M. Liu, *et al.*, Additive manufacturing of nanocellulose/polyborosilazane derived CNFs-SiBCN ceramic metamaterials for ultra-broadband electromagnetic absorption, *Chem. Eng. J.*, 433(2022), art. No. 133743.
- [38] Q.Q. Huang, G.H. Wang, M. Zhou, J. Zheng, S.L. Tang, and G.B. Ji, Metamaterial electromagnetic wave absorbers and devices: Design and 3D microarchitecture, *J. Mater. Sci. Technol.*, 108(2022), p. 90.
- [39] F.K. Zhou, R.Y. Tan, W. Fang, *et al.*, An ultra-broadband microwave absorber based on hybrid structure of stereo metamaterial and planar metasurface for the S, C, X and Ku bands, *Results Phys.*, 30(2021), art. No. 104811.
- [40] Q. Zhou, B. Xue, S.Y. Gu, F. Ye, X.M. Fan, and W.Y. Duan, Ultra broadband electromagnetic wave absorbing and scattering properties of flexible sandwich cylindrical water-based metamaterials, *Results Phys.*, 38(2022), art. No. 105587.
- [41] Y.Q. Zhang, H.X. Dong, N.L. Mou, H.N. Li, X. Yao, and L. Zhang, Tunable and transparent broadband metamaterial absorber with water-based substrate for optical window applications, *Nanoscale*, 13(2021), No. 16, p. 7831.
- [42] Y.X. Li, Y.G. Duan, and X.Q. Kang, Multi-scale integrated design and fabrication of ultrathin broadband microwave absorption utilizing carbon fiber/Prussian blue/Fe₃O₄-based lossy lattice metamaterial, *J. Mater. Chem. C*, 9(2021), No. 19, p. 6316.
- [43] X.X. Sun, Y.B. Li, Y.X. Huang, Y.J. Cheng, S.S. Wang, and W.L. Yin, Achieving super broadband electromagnetic absorption by optimizing impedance match of rGO sponge metamaterials, *Adv. Funct. Mater.*, 32(2022), No. 5, art. No. 2107508.
- [44] S.S. Kim, S.B. Jo, K.I. Gueon, K.K. Choi, J.M. Kim, and K.S. Churn, Complex permeability and permittivity and microwave absorption of ferrite-rubber composite at X-band frequencies, *IEEE Trans. Magn.*, 27(1991), No. 6, p. 5462.
- [45] W. Li, T.L. Wu, W. Wang, P.C. Zhai, and J.G. Guan, Broadband patterned magnetic microwave absorber, *J. Appl. Phys.*, 116(2014), No. 4, art. No. 044110.
- [46] Y.X. Huang, X.J. Yuan, M.J. Chen, *et al.*, Ultrathin flexible carbon fiber reinforced hierarchical metastructure for broadband microwave absorption with nano lossy composite and multiscale optimization, *ACS Appl. Mater. Interfaces*, 10(2018), No. 51, p. 44731.
- [47] D.R. Smith, D.C. Vier, T. Koschny, and C.M. Soukoulis, Electromagnetic parameter retrieval from inhomogeneous metamaterials, *Phys. Rev. E*, 71(2005), No. 3, art. No. 036617.
- [48] P.Y. Liu, L.M. Wang, B. Cao, *et al.*, Designing high-performance electromagnetic wave absorption materials based on polymeric graphene-based dielectric composites: From fabrication technology to periodic pattern design, *J. Mater. Chem. C*, 5(2017), No. 27, p. 6745.
- [49] K.L. Zhang, J.Y. Zhang, Z.L. Hou, S. Bi, and Q.L. Zhao, Multifunctional broadband microwave absorption of flexible graphene composites, *Carbon*, 141(2019), p. 608.
- [50] Z.C. Lou, X. Han, J. Liu, *et al.*, Nano-Fe₃O₄/bamboo bundles/phenolic resin oriented recombination ternary composite with enhanced multiple functions, *Composites Part B*, 226(2021), art. No. 109335.